Original Article

KMT2C expression and DNA homologous recombination repair factors in lung cancers with a high-grade fetal adenocarcinoma component

Masaki Suzuki[1,2], Rika Kasajima[3,4], Tomoyuki Yokose[2], Eigo Shimizu[4], Seira Hatakeyama[5], Kiyoshi Yamaguchi[5], Kazuaki Yokoyama[6], Kotoe Katayama[4], Rui Yamaguchi[4,7,8], Yoichi Furukawa[5], Satoru Miyano[4,9], Seiya Imoto[4], Aya Shinozaki-Ushiku[1], Tetsuo Ushiku[1], Yohei Miyagi[3]

[1]Department of Pathology, The University of Tokyo, Tokyo, Japan; [2]Department of Pathology, Kanagawa Cancer Center, Yokohama, Japan; [3]Molecular Pathology and Genetics Division, Kanagawa Cancer Center Research Institute, Yokohama, Japan; [4]Division of Health Medical Intelligence, Human Genome Center, Institute of Medical Science, The University of Tokyo, Tokyo, Japan; [5]Division of Clinical Genome Research, Institute of Medical Science, The University of Tokyo, Tokyo, Japan; [6]Department of Hematology/Oncology, Research Hospital, Institute of Medical Science, The University of Tokyo, Tokyo, Japan; [7]Division of Cancer Systems Biology, Aichi Cancer Center Research Institute, Nagoya, Japan; [8]Division of Cancer Informatics, Nagoya University Graduate School of Medicine, Nagoya, Japan; [9]Department of Integrated Data Science, Medical and Dental Data Science Center, Tokyo Medical and Dental University, Tokyo, Japan

Contributions: (I) Conception and design: M Suzuki, R Kasajima, Y Miyagi; (II) Administrative support: T Yokose; (III) Provision of study materials or patients: M Suzuki, T Yokose; (IV) Collection and assembly of data: M Suzuki, R Kasajima; (V) Data analysis and interpretation: All authors; (VI) Manuscript writing: All authors; (VII) Final approval of manuscript: All authors.

Correspondence to: Yohei Miyagi, MD. Molecular Pathology and Genetics Division, Kanagawa Cancer Center Research Institute, 2-3-2 Nakao, Asahi-ku, Yokohama-city, Kanagawa 241-8515, Japan. Email: miyagi@gancen.asahi.yokohama.jp.

Background: High-grade fetal adenocarcinoma of the lung (H-FLAC) is a rare variant of pulmonary adenocarcinoma. Our previous study showed a high frequency of KMT2C mutations in lung cancers with an H-FLAC component, showing that KMT2C dysfunction may be associated with the biological features of H-FLACs.

Methods: In this study, we performed RNA sequencing and immunohistochemical analysis to identify the differentially expressed genes and corresponding pathways associated with H-FLACs, compared with common adenocarcinomas.

Results: Ingenuity pathway analysis based on RNA sequencing data revealed that DNA homologous recombination repair (HRR) pathways were significantly inactivated in H-FLAC. Expression of *KMT2C*, *ATM*, *ATR*, and *BRCA2* was significantly lower in H-FLACs than in common adenocarcinomas, and *BRCA1* expression showed a decreasing trend. Pearson correlation analyses for all cases revealed that *KMT2C* expression showed a strong positive correlation (R>0.7) with the expression of *ATR*, *BRCA1*, and *BRCA2* genes and a moderately positive correlation with *ATM* expression (R=0.47). Immunohistochemical analysis showed significantly lower levels of KMT2C, ATM, ATR, and BRCA2 expression in H-FLACs than in common adenocarcinomas, and a trend of lower BRCA1 levels. Additionally, KMT2C expression showed a weak to moderate correlation with that of ATM, ATR, BRCA1, and BRCA2.

Conclusions: Cancers containing H-FLAC components showed lower levels of KMT2C and HRR factors than common lung adenocarcinomas, and their levels exhibited a positive correlation. These results support the hypothesis that loss of KMT2C function decreases the expression of the HRR factors in H-FLACs. H-FLACs with low *KMT2C* expression may be a good indication for poly (ADP-ribose) polymerase (PARP) inhibitor-based therapy.

Keywords: Fetal adenocarcinoma; KMT2C; lung adenocarcinoma; BRCA1; BRCA2

Submitted Mar 03, 2023. Accepted for publication Jul 20, 2023. Published online Aug 16, 2023.
doi: 10.21037/tlcr-23-137
View this article at: https://dx.doi.org/10.21037/tlcr-23-137

Introduction

Background

Fetal adenocarcinoma of the lung is a rare variant of lung adenocarcinoma, displaying characteristic histology resembling the fetal lung epithelium of the pseudoglandular stage, and is classified into low-grade and high-grade forms (1,2). Low-grade fetal lung adenocarcinoma (L-FLAC) frequently occurs in young- to middle-aged women with a smoking history, and its histology often shows morule formation (1,3). High-grade fetal adenocarcinoma (H-FLAC) predominantly occurs in elderly men with a history of heavy smoking and histologically shows marked nuclear atypia and no morule formation (1,4-7). H-FLAC usually coexists with other components such as common adenocarcinoma, enteric adenocarcinoma, and neuroendocrine carcinoma (4,6,7). Similar to micropapillary adenocarcinomas, lung adenocarcinomas with an H-FLAC component have poor prognoses (7). L-FLAC recurrently exhibits mutations of *CTNNB1* and *DICER1*, which are rare in H-FLACs (8-10). Therefore, L- and H-FLACs have diverse clinicopathological and molecular features and may develop through distinct tumorigenic pathways (1,6,11).

Highlight box

Key findings

- High-grade fetal adenocarcinoma (H-FLAC) components showed lower expression of *KMT2C* and homologous recombination repair (HRR) factors than common lung adenocarcinomas.
- *KMT2C* expression was positively correlated with the expression of HRR factors.

What is known and what is new?

- Only two studies using cancer cell lines previously reported that *KMT2C* directly and/or indirectly promotes the expression of HRR factors, and *KMT2C* dysfunction was associated with sensitivity to PARP inhibitors.
- KMT2C expression was significantly lower in surgically resected H-FLACs than in that of common adenocarcinomas.

What is the implication, and what should change now?

- H-FLACs with a high degree of *KMT2C* dysfunction may be highly sensitive to PARP inhibitors. PARP inhibitors should only be considered for treatment of H-FLAC after further studies.

Our recent study (11) showed that lung cancers with H-FLAC components rarely harboured druggable driver gene mutations but exhibited a high frequency of *KMT2C* mutations (6/16 cases, 38%). *KMT2C* encodes a histone H3K4 monomethyltransferase, and its expression leads to enhancer activation (12). Although little is known about the consequences of *KMT2C* dysfunction in cancer cells, Rampias *et al.* recently reported that low *KMT2C* activity in bladder cancer cells is associated with a decrease in *ATM*, *ATR*, *BRCA1*, and *BRCA2* expression, resulting in the impairment of homologous recombination-mediated DNA double-strand break repair and high sensitivity to olaparib, a poly (ADP-ribose) polymerase (PARP1/2) inhibitor (13). PARP1 and PARP2 are enzymes involved in the DNA damage response and facilitate DNA single-strand break repair (14). PARP1/2 inhibitors lead to genomic instability and cell death in tumour cells with mutations in *BRCA1/2* genes, which encode proteins involved in key stages of homologous recombination in DNA double-strand break repair (15).

In the past few decades, platinum-based cytotoxic chemotherapy has been the systemic treatment of choice for unresectable advanced lung cancers. Currently, targeted molecular therapy for lung cancers is rapidly developing, and various kinase inhibitors are used clinically to treat non-small-cell lung cancers with targetable driver mutations of *EGFR*, *ALK*, *RET*, *ROS1*, *BRAF*, and *MET* genes (16). First-line immunotherapy with a PD-L1 checkpoint inhibitor also represents a marked development in the treatment of advanced non-small-cell lung cancers with high PD-L1 levels and no driver mutations (17). The lack of targetable driver mutations causes most cases of H-FLACs to be ineligible for current targeted molecular therapy with kinase inhibitors. Additionally, H-FLACs tend to have no/low PD-L1 expression; therefore, immunotherapy may also have little effect on H-FLAC cases (11).

Rationale and knowledge gap

As H-FLACs harbour a high frequency of *KMT2C* mutations, epigenetic aberrations due to KMT2C dysfunction seemed to be associated with the biological features of H-FLACs. *KMT2C* dysfunction in H-FLACs

may lead to impaired DNA damage repair through homologous recombination and PARP1/2 inhibitor sensitization. However, there are few studies on the expression and functional consequences of KMT2C in non-small cell lung cancer tissues. To our knowledge, the effect of KMT2C aberration on H-FLACs has not been investigated yet.

Objective

To investigate the functional consequences of *KMT2C* expression in H-FLAC, we first obtained an RNA expression profile by RNA sequencing and identified differentially expressed genes and pathways between H-FLAC and common primary lung adenocarcinomas. Next, we focused on homologous recombination repair (HRR) factors, such as ATM, ATR, BRCA1, and BRCA2, and performed immunohistochemical analysis of HRR factors to evaluate the levels of protein expression in H-FLAC and common adenocarcinomas and then examined the association between KMT2C and HRR factor expression in H-FLAC. Additionally, we focused on RAD51 which is another critical effector of HRR factor (18) and investigated RAD51 expression in H-FLAC. We present this article in accordance with the STROBE reporting checklist (available at https://tlcr.amegroups.com/article/view/10.21037/tlcr-23-137/rc).

Methods

Case selection

The study was conducted in accordance with the Declaration of Helsinki (as revised in 2013). The study was approved by the ethics committee of the Kanagawa Cancer Center (approval No. H28-Res60) in Yokohama, Japan, and individual consent for this retrospective analysis was waived. We obtained 16 cases (F1–F16) of surgically resected primary lung cancers with an H-FLAC components present in various proportions (at least 5% of the total tumour volume). All cases were previously reported (11). The case numbers of lung cancers with an H-FLAC component were the same as those in the previous report, and KMT2C mutations were detected in F4, F5, F8, F10, F12, and F13 in the previous study (11). H-FLAC was histologically defined as previously described (7). Additionally, for comparative analyses, we collected common primary lung adenocarcinomas, which were surgically resected at the Kanagawa Cancer Center, and randomly selected 16 cases (C1–C16) that were matched with the H-FLAC cases by clinicopathological factors such as age, sex, smoking status, pathological stage, and year of operation. The common adenocarcinoma cases selected consisted of non-mucinous neoplastic glands with a complex admixture of histologic patterns (lepidic, acinar, papillary, micropapillary, and solid) and lacked components of special variants, including invasive mucinous, colloid, fetal, and enteric-type adenocarcinomas. All resected tissues were fixed in 10% formalin, embedded in paraffin, and stained with haematoxylin and eosin (HE). Histological assessment and classification were performed following the World Health Organization classification of lung tumours (2). Although the Union for International Cancer Control (UICC) published the 8th edition of the UICC TNM classification of malignant tumours in 2017 (19), the lung cancer stages in this study were evaluated using the 7th edition (20), owing to the difficulty in the accurate retrospective measurement of invasive sizes of past lung cancer cases.

RNA sequencing

Based on the area of tumour tissues in the HE-stained section, total RNA was isolated from formalin-fixed paraffin-embedded tumour tissues of each lung cancer case (F1–16 and C1–16) and subjected to transcriptome analysis by RNA sequencing. In the H-FLAC cases (F1–16), tissues from only the H-FLAC components were manually obtained through macrodissection and used for the analysis. Total RNA was extracted using a NucleoSpin totalRNA FFPE XS kit (Macherey-Nagel GmbH & Co. KG, Germany), according to the manufacturer's instructions. The purity of the isolated RNA was evaluated with optical density ratios (A_{260}/A_{280} and A_{260}/A_{230}), using the NanoPhotometer (Implen, Munich, Germany). The RNA integrity was assessed with RNA integrity numbers (RIN) and DV200 using the RNA Nano 6000 Assay Kit and Agilent Bioanalyzer 2100 system (Agilent Technologies, Santa Clara, CA, USA). Library synthesis was performed on samples with DV200 greater than 20%. The RNA sequencing library was constructed using the TruSeq RNA Access Library Kit (Illumina, San Diego, CA, USA), followed by sequencing using the HiSeq2500 sequencing system (Illumina).

Analysis of RNA sequencing data

We used FastQC (https://www.bioinformatics.babraham.

ac.uk/projects/fastqc/) to confirm the read quality. Alignment to the human genome GRCh37 was performed using STAR-2.5.2a (https://github.com/alexdobin/STAR/releases/tag/2.5.2a), and quality assessment of the binary-sequence alignment map (BAM) for each sample was performed using the Genomon 2 RNA analysis pipeline (https://github.com/Genomon-Project) at the Human Genome Center, the Institute of Medical Science, University of Tokyo (Tokyo, Japan). The mapped read count for each sample was calculated using HTseq (https://htseq.readthedocs.io/en/release_0.9.1/) and normalised. The obtained read count data of genes were subjected to principal component analysis (PCA), and identification of the differentially expressed genes (DEGs) between the groups was performed using "DESeq2" Bioconductor R package (v1.26.0; http://www.bioconductor.org/packages/release/bioc/vignettes/DESeq2/inst/doc/DESeq2.html).

The ingenuity pathway analysis (IPA; Ingenuity Systems, Redwood City, CA, USA) was used to identify and understand the biological significance of the pathways involving the DEG products. The IPA interrogated the identified DEGs as "focus genes" against genes curated in their ingenuity knowledge database based on functional annotations and experimental observations.

The correlations of mRNA expression for genes were estimated by Pearson correlation analysis. The RNA sequencing read count data for each gene, normalised using the "Relative Log Expression (RLE)" method implemented in the "DESeq2" R package (v1.26.0), were used to calculate the correlation coefficient (R) between genes using the statistical programming environment R 4.0.3 (R Project for Statistical Computing, Vienna, Austria. https://www.R-project.org/).

External datasets for RNA sequencing of lung adenocarcinomas

We obtained fastq files of RNA sequencing for 463 lung adenocarcinomas from The Cancer Genome Atlas (TCGA) under an authorized account. The data were analysed using the Genomon 2 RNA analysis pipeline as our original RNA sequencing data described above.

Immunohistochemical analysis

Immunohistochemical staining was performed for the formalin-fixed paraffin-embedded tissue sections using an automated immunostainer (Histostainer 48A; Nichirei, Tokyo, Japan) with the following primary antibodies at respective dilutions: anti-KMT2C (Millipore Cat# ABE1851, dilution 1:300), anti-ATM (Abcam Cat# ab32420, RRID: AB_725574, dilution 1:100), anti-ATR (LSBio Cat# LS B4288-50, RRID: AB_10945735, dilution 1:50), anti-BRCA1 (Abcam Cat# ab16780, RRID: AB_2259338, dilution 1:200), anti-BRCA2 (Sigma-Aldrich Cat# HPA026815, RRID: AB_10602692, dilution 1:50), and anti-RAD51 (Abcam Cat# ab16780, RRID: AB_2722613, dilution 1:200). EnVison Flex+ Mouse LINKER (Agilent Technologies, Santa Clara, CA, USA) was added to amplify the signal of the anti-ATR antibody. The expression of each marker was detected using the Histofine Simple Stain MAX-PO (M) or (R) kits (Nichirei, Tokyo, Japan). Appropriate positive and negative control tissues were used in each experiment. Each staining was classified by a score from 0 to 3+ based on the proportion and intensity of the immunoreactive tumour cells (score 0: absent or weak nuclear expression in <50% of tumour cells, score 1+: weak nuclear expression in ≥50% of tumour cells, score 2+: moderate nuclear expression in ≥50% of tumour cells, and score 3+: strong nuclear expression in ≥50% of tumour cells).

Statistical analyses

The threshold value to identify the DEGs was a greater than 2-fold change in expression, with a P value <0.05 and an adjusted P value <0.05. In IPA analysis, we evaluated the probability of the identified pathways by calculating the P-value using the right-tailed Fisher's exact test, and pathways with a P value <0.05 were considered significant. Additionally, z-scores were automatically calculated by the IPA, and positive and negative z-scores indicated activation and inactivation of pathways, respectively. Z-scores for pathways involving DEGs without enough information regarding their biological significance in the IPA dataset were ineligible for assignment and were designated as NaN.

The Mann-Whitney U test was performed to compare the scores of immunohistochemical analysis. Spearman's correlation analysis was performed to examine the correlation between the immunohistochemical scores of KMT2C and each HRR factor. The correlation strength with respect to the correlation coefficient was determined as follows: very weak correlation at $|r|<0.2$, weak correlation at $0.2\leq|r|<0.4$, moderate correlation at $0.4\leq|r|<0.6$, strong correlation at $0.6\leq|r|<0.8$, and very strong correlation at $0.8\leq|r|$. In all statistical tests, P values <0.05 were considered significant. Statistical analyses were performed using EZR (Easy R)

Table 1 Clinicopathological features of lung cancers with a fetal component and common adenocarcinomas

Features	Lung cancers with H-FLAC	Common adenocarcinomas
Total number (n)	16	16
Age (year)		
Median	67	68
Range	52–81	55–78
Sex		
Female	3	3
Male	13	13
Smoking		
Never	2	2
Ever	14	14
Stage		
IA	3	3
IB	5	5
IIA	3	3
IIB	2	2
IIIA	3	3

H-FLAC, high-grade fetal adenocarcinoma.

statistical software, version 1.36 (Saitama Medical Center, Jichi Medical University, Saitama, Japan) and a graphical user interface for R (The R Foundation for Statistical Computing, Vienna, Austria).

Results

Clinicopathological features

The clinicopathological findings for the lung cancer cases with and without an H-FLAC component are summarised in *Table 1*. In the cases with a H-FLAC component, columnar clear cells formed glandular, cribriform, and/or papillary structures with pseudostratified atypical nuclei, displaying a "piano keyboard-like" appearance (*Figure 1*). The H-FLAC components existed in various proportions: 5–9% in one case; 10–19% in two cases; 50–59% in one case; 60–69% in four cases; 70–79% in three cases; 80–89% in one case; 90–99% in two cases; and 100% in two cases. The predominant histology of the common lung adenocarcinoma cases was as follows: lepidic in two cases, acinar in five cases, papillary in seven cases, and solid in two cases.

Transcriptome analysis using PCA, DESeq2, and IPA

RNA samples from 15 H-FLAC and all 16 common adenocarcinoma counterparts passed the quality inspection and were subjected to RNA sequencing. All the sequencing data acquired for each sample had an average of more than 25 million reads, and the quality of sequencing was over Q30, which was confirmed using FastQC. Differences in gene expression profile were first analysed by PCA (Figure S1), where H-FLAC was clearly distinguished from common adenocarcinoma regardless of an H-FLAC component ratio similar to the total tumour volume.

DESeq2 analysis identified 2112 genes that were significantly differentially expressed in H-FLAC and common adenocarcinoma. All DEGs identified are shown in available online: https://cdn.amegroups.cn/static/public/tlcr-23-137-1.xlsx. The DEGs were then used to identify the significant biological pathways associated with H-FLAC in comparison with common adenocarcinoma. Forty-six pathways were identified, 32 of which were inactivated in H-FLAC, 3 were activated, and the remaining 11 pathways were not assigned to either direction based on the z-score (Table S1). The pathway most significantly associated with H-FLAC was the "role of BRCA1 in DNA damage response", which was inactivated in H-FLAC (*Figure 2*). Notably, multiple pathways related to DNA damage responses and cell cycle checkpoint regulations were significantly associated with H-FLAC. The pathways "ATM signalling" and "role of CHK proteins in cell cycle checkpoint control" were inactivated, whilst the pathways "G2/M DNA damage checkpoint regulation" and "p53 signalling" were activated (*Figure 2*, Figure S2). Although the direction of activation-inactivation was not assigned, the pathways "hereditary breast cancer signalling" and "DNA double-strand break repair by homologous recombination" showed significant association with H-FLAC, due to the DEGs involved in these pathways (*Figure 2*, Table S1). In addition to the DNA damage/cell cycle regulation-related pathways, multiple pathways related to small GTPases such as "RhoA signalling," "Rac signalling," and "signalling by Rho family GTPases" were inactivated in H-FLAC (*Figure 2*). Consistent with the inactivation of Rho/Rac signalling pathways, pathways "actin cytoskeleton

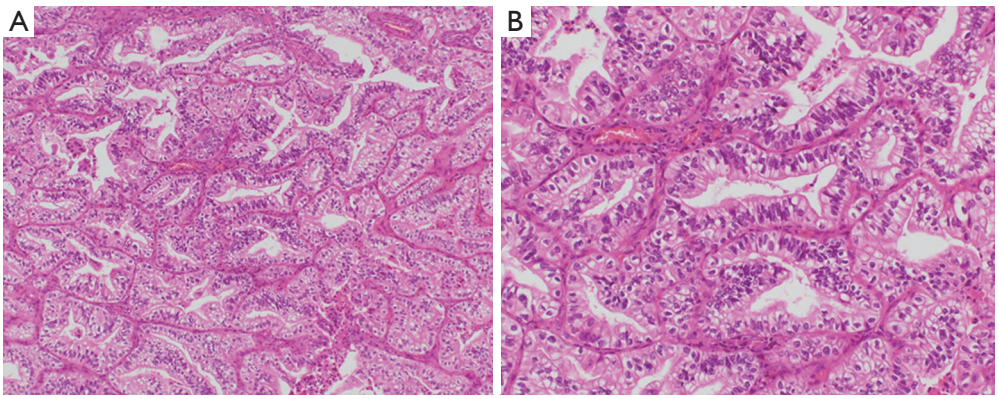

Figure 1 Histology of lung cancer with a H-FLAC component. H-FLAC component exhibited complex glandular structures (A) composed of columnar cells with clear cytoplasm and pseudostratified nuclei, displaying a "piano keyboard-like appearance" (B). Staining method: haematoxylin and eosin stain. Magnification: ×100 (A), ×200 (B). H-FLAC, high-grade fetal adenocarcinoma.

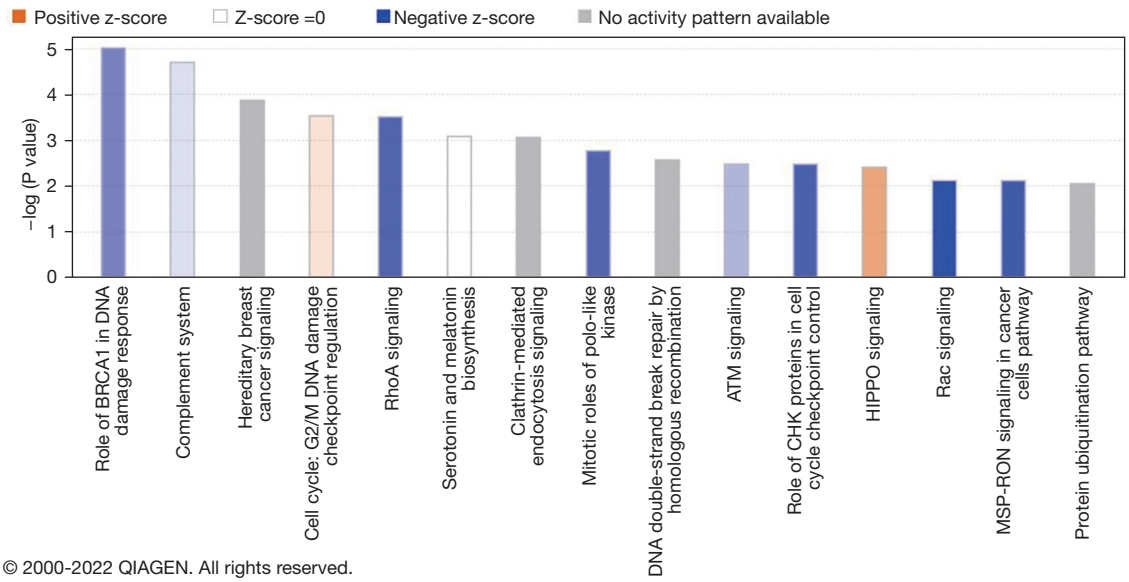

Figure 2 Biological pathways associated with differentially expressed genes in H-FLAC components. The significant pathways identified by IPA analysis for the DEGs in H-FLAC and the common adenocarcinoma counterpart are depicted. The y-axis displays the –log of the P value calculated by the right-tailed Fisher's Exact Test, and the height of each bar indicates the probability of the association. Only the pathways with –log (P value) greater than 2 (corresponding to a P value less than 0.01) were depicted in this figure. Blue bars indicate the pathways inactivated in H-FLAC and orange ones indicate pathways activated in H-FLAC. White bars represent unpredicted pathway activation/inhibition. Gray bars indicate those that are ineligible for activity prediction analysis. The title of the pathway is shown on the x-axis. The drawing was made through the IPA analysis, provided by the Ingenuity systems, QIAGEN. H-FLAC, high-grade fetal adenocarcinoma; IPA, ingenuity pathway analysis; DEGs, differentially expressed genes.

signalling" and "paxillin signalling" were also inactivated in H-FLAC (*Figure 2*). Pathways with P values less than 0.01 [corresponding to –log (P value) greater than 2] are depicted in *Figure 2*. All the significant pathways are listed in Table S1 and are depicted in Figure S2.

We further analysed DEGs between six H-FLACs with *KMT2C* mutation and nine without mutations. Nineteen genes were identified as DEGs and their IPA analysis only found one pathway, nNOS (neuronal nitric oxides synthase) signalling in skeletal muscle cell without activity pattern (Figure S3A).

KMT2C expression and HRR genes in H-FLAC

KMT2C expression in H-FLAC was significantly lower (less than a half) than that in common adenocarcinomas (log2 fold change =−1.09, P=1×10^{-4}, available online: https://cdn.amegroups.cn/static/public/tlcr-23-137-1.xlsx). The expression of *KMT2C*, *ATM*, *ATR*, and *BRCA2* was significantly lower in H-FLAC than in common adenocarcinomas (*Figure 3A*). Pearson correlation analysis for all cases revealed that *KMT2C* expression showed a strong positive correlation with *ATR*, *BRCA1*, and *BRCA2* expression [correlation coefficient (R) greater than 0.7], and a moderately positive correlation with *ATM* expression (R=0.47; *Figure 3B*). Although H-FLAC did not show significant correlation between *KMT2C* and the expression of any of the HRR factors examined (*Figure 3C*), *KMT2C* expression showed a strong positive correlation with *ATR*, *BRCA1*, and *BRCA2* expression in common adenocarcinomas (*Figure 3D*). Furthermore, the positive correlation between *KMT2C* and HRR genes *ATM*, *ATR*, and *BRCA1* was observed in the 463 TCGA lung adenocarcinoma cases.

We further compared the expression of *ATM*, *ATR*, *BRCA1*, and *BRCA2* in six H-FLACs with *KMT2C* mutation and nine without mutations. No genes showed significantly different expression between the two groups (Figure S3B).

Immunohistochemical analysis for KMT2C expression and HRR factors

The immunohistochemical features are displayed in *Figures 4,5*. In the F1, F3, F7, and F9 cases, non-fetal-type components could not be evaluated because the tumours were almost entirely comprised of H-FLAC components (*Figure 4*). Low KMT2C expression with a score of 1+ was identified in more H-FLAC components than in common adenocarcinomas (*Figures 4,5A*), and H-FLACs showed significantly lower KMT2C expression than in common adenocarcinomas (*Table 2*, Figure S4). Some cases showed lower KMT2C expression in the H-FLAC component than in the non-fetal-type component, although there were no significant differences between them (*Table 2*). Additionally, expression of HRR factors except RAD51 tended to be lower in H-FLAC components than in common adenocarcinomas (*Figures 4,5B-5D*), and ATM, ATR, and BRCA2 expression was significantly lower in H-FLAC components than in common adenocarcinomas (*Table 2*, Figure S4). Low nuclear expression (score 0 or 1+) of RAD51 was observed in 12/16 cases of H-FLACs and 12/16 cases of common adenocarcinomas (*Figures 4,5F*). Only one case (F7) showed cytoplasmic RAD51 expression. As the difference between the expression of fetal and non-fetal components of H-FLAC cases was unclear, only images of fetal components of the H-FLAC cases and cancer tissues of the common adenocarcinomas are shown in *Figure 5*.

Next, we examined the correlation of the immunohistochemical scores between KMT2C and each HRR factor for all cases using Spearman's correlation. The correlation coefficients between KMT2C and HRR factors were 0.553 (P=0.001) for ATM, 0.445 (P=0.01) for ATR, 0.378 (P=0.03) for BRCA1, 0.423 (P=0.02) for BRCA2, 0.117 (P=0.52) for RAD51. ATM, ATR, and BRCA2 expression moderately correlated with KMT2C expression, and BRCA1 expression weakly correlated with KMT2C expression. RAD51 expression showed no significant correlation with KMT2C expression. In the correlation analysis of H-FLACs or common adenocarcinomas, there was no significant correlation between the immunohistochemical scores of KMT2C and any of the HRR factors.

Discussion

Key findings

Our previous study identified missense or nonsense *KMT2C* mutations in six out of the 16 H-FLAC cases (38%) examined, whereas 14% of common lung adenocarcinomas harboured mutations in *KMT2C* according to the TumorPortal (http://www.tumorportal.org/) (11). Based on these findings, we surmised that *KMT2C* aberration may be a characteristic of H-FLAC. In this study, we revealed that both mRNA and protein expression of *KMT2C* were attenuated in H-FLAC. Further, HRR pathways were identified as significantly inactivated in H-FLACs by Ingenuity pathway analysis. Accordingly, the RNA and protein expression of *ATM*, *ATR*, and *BRCA2* was significantly lower in H-FLAC components than in common adenocarcinomas. In addition, *KMT2C* expression was strongly correlated with that of *ATR*, *BRCA1*, and *BRCA2* and was moderately correlated with that of *ATM* in adenocarcinomas together with H-FLAC and common adenocarcinoma or in common adenocarcinoma alone. The correlated expression of *KMT2C* and HRR genes examined seemed to be a characteristic of adenocarcinoma of the lung including ones with H-FLAC components.

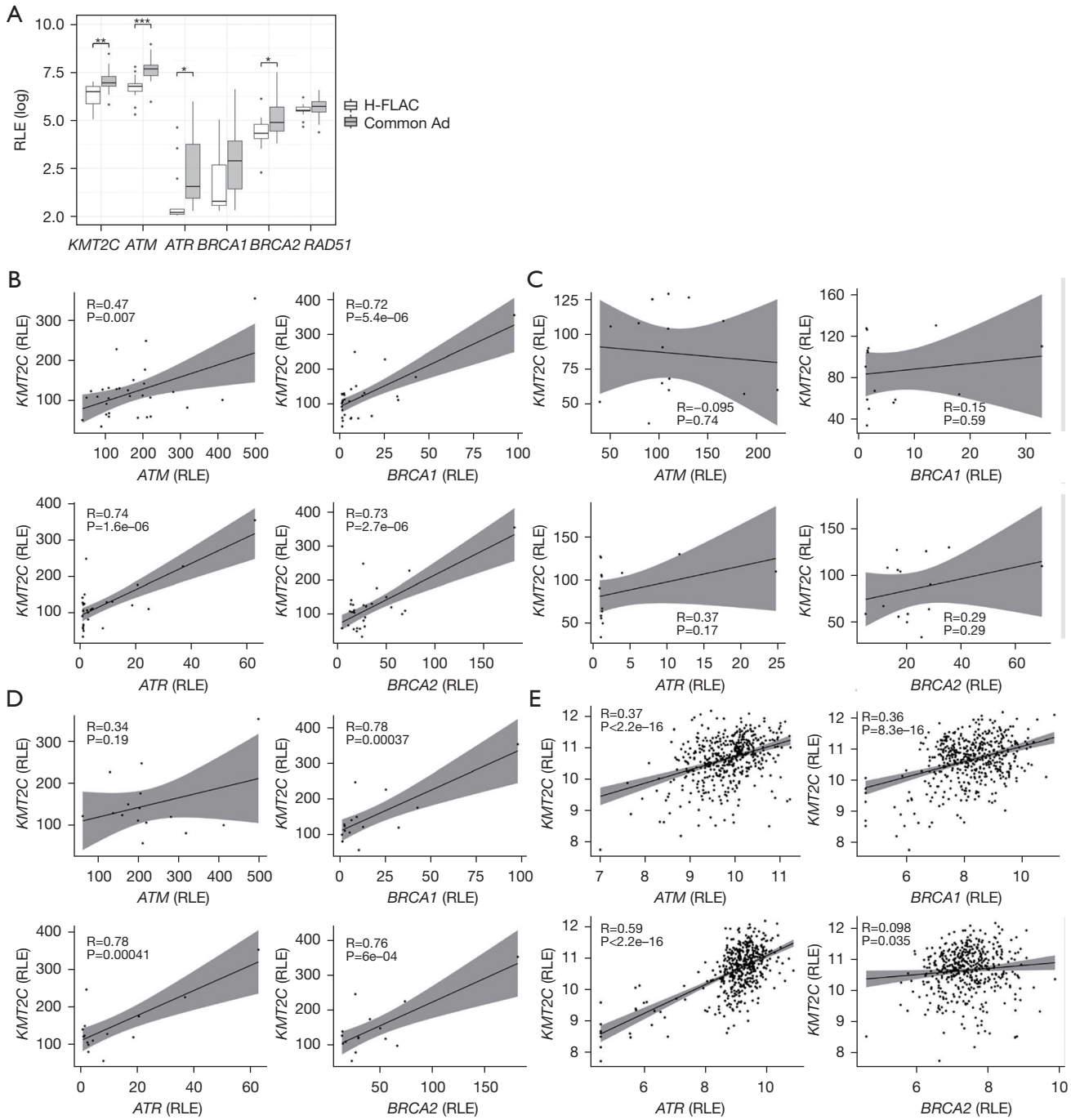

Figure 3 Expression of *KMT2C* in relation to *ATM*, *ATR*, *BRCA1*, *BRCA2*, and *RAD51*. (A) Expression of *KMT2C*, *ATM*, *ATR*, *BRCA1*, *BRCA2*, and *RAD51* was compared between H-FLAC and common adenocarcinomas (common Ad). Boxes indicate the first and the third quartile counts, lines in boxes indicate median values, and ends of whiskers indicate minimum and maximum values, respectively. Dots demonstrate outliers. (B-E) Pearson correlation analysis for the expression of *KMT2C* and *ATM*, *ATR*, *BRCA1*, and *BRCA2* genes in all cases (B), only in H-FLAC cases (C), only in common adenocarcinoma cases (D), and in TCGA lung adenocarcinoma cases (E). The x-axis and y-axis indicate the value of RLE normalised RNA read counts of each gene (B-D). The x-axis and y-axis indicate the $\log_2$ value of RLE normalised RNA read counts of each gene (E). *, P<0.05; **, P<0.01; ***, P<0.001. R indicates the correlation coefficient. H-FLAC, high-grade fetal adenocarcinoma; RLE, Relative Log Expression; TCGA, The Cancer Genome Atlas.

Case	KMT2C		ATM		ATR		BRCA1		BRCA2		RAD51	
	H-FLAC	nonH-FLAC	H-FLAC	nonH-FLAC	H-FLAC	nonH-FLAC	H-FLAC	nonH-FLAC	H-FLAC	nonH-FLAC	H-FLAC	nonH-FLAC
F1	1+		1+		1+		2+		1+		1+	
F2	1+	2+	2+	2+	1+	2+	1+	2+	1+	2+	0	1+
F3	2+		2+		2+		2+		1+		0	
F4	1+	1+	3+	3+	2+	2+	2+	3+	2+	3+	0	1+
F5	2+	2+	2+	2+	2+	2+	1+	3+	1+	2+	0	0
F6	1+	2+	1+	1+	3+	3+	2+	1+	1+	1+	1+	2+
F7	1+		2+		3+		2+		2+		2+	
F8	1+	1+	2+	2+	1+	2+	2+	2+	1+	1+	2+	1+
F9	1+		2+		1+		2+		2+		1+	
F10	2+	3+	2+	2+	2+	2+	2+	3+	2+	2+	1+	1+
F11	2+	2+	1+	1+	1+	1+	1+	1+	1+	2+	1+	2+
F12	2+	2+	2+	2+	2+	3+	2+	2+	1+	2+	2+	2+
F13	3+	3+	3+	2+	3+	3+	3+	2+	1+	2+	2+	2+
F14	3+	3+	2+	3+	3+	3+	2+	2+	2+	2+	1+	1+
F15	3+	3+	3+	3+	2+	3+	3+	3+	2+	2+	0	2+
F16	2+	2+	2+	2+	2+	3+	1+	2+	1+	1+	1+	2+
C1		3+		3+		2+		1+		2+		0
C2		3+		3+		3+		2+		2+		1+
C3		2+		2+		2+		1+		2+		1+
C4		3+		3+		3+		3+		3+		2+
C5		3+		3+		2+		3+		3+		1+
C6		3+		3+		3+		2+		1+		1+
C7		2+		2+		2+		2+		1+		1+
C8		2+		3+		3+		2+		1+		1+
C9		1+		3+		2+		2+		1+		1+
C10		3+		3+		2+		3+		3+		2+
C11		3+		3+		2+		3+		2+		2+
C12		2+		0		3+		2+		1+		1+
C13		3+		3+		3+		2+		2+		2+
C14		1+		2+		2+		2+		2+		1+
C15		2+		2+		3+		3+		3+		0
C16		3+		2+		3+		2+		3+		0

Figure 4 Immunohistochemical features of the lung cancers with and without the fetal components. The two boxes for each molecular marker represent the immunohistochemical scores. The boxes on the left show the immunohistochemical score of the H-FLAC component. The boxes on the right show the immunohistochemical score of the nonH-FLAC component. F1-16 are H-FLAC cases and C1-16 are common adenocarcinoma cases. F1, F3, F7, and F9 were almost entirely comprised of H-FLAC components and could not be evaluated in non-fetal-type components (shown in a slant line). Low expression (score 0 or 1+), intermediate expression (score 2+) and high expression (score 3+) were coloured blue, white and red, respectively. H-FLAC, high-grade fetal adenocarcinoma.

Strengths and limitations

We analysed a cohort of rare lung cancer cases with H-FLAC components. To our knowledge, this is the first comprehensive expression analysis of H-FLAC cases. However, this study did have some limitations. The first issue is that we used a small control cohort of common lung adenocarcinoma cases for comparative analyses with H-FLAC. Although using a large-scale cohort is preferred, most publicly available expression datasets of lung adenocarcinomas (such as TCGA) are derived from frozen tissues instead of formalin-fixed paraffin-embedded tissues, and it was difficult to adopt such datasets for this study. Therefore, we used the control cohort of 16 cases (the same number of H-FLAC cases) that were matched based on clinicopathological factors. If more cases could have been analysed, a significant correlation between expressions of *KMT2C* and HRR factors might have been obtained after dividing the group into H-FLACs and common adenocarcinomas. However, due to the rarity of H-FLACs and the cost of analysis, it was difficult to increase the number of cases. The second is that we did not observe differences between H-FLAC with and without *KMT2C* mutations in expression of *KMT2C* and HRR

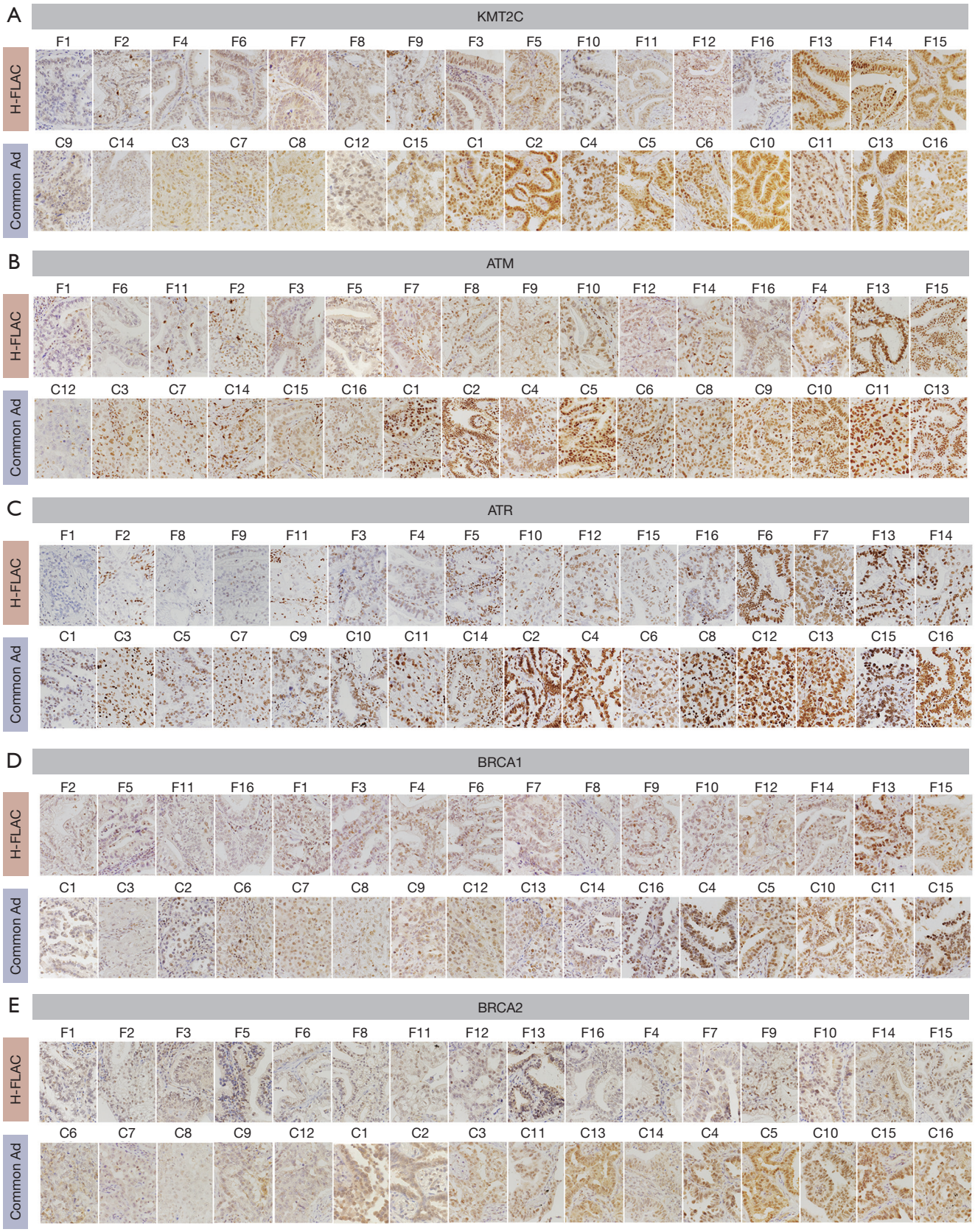

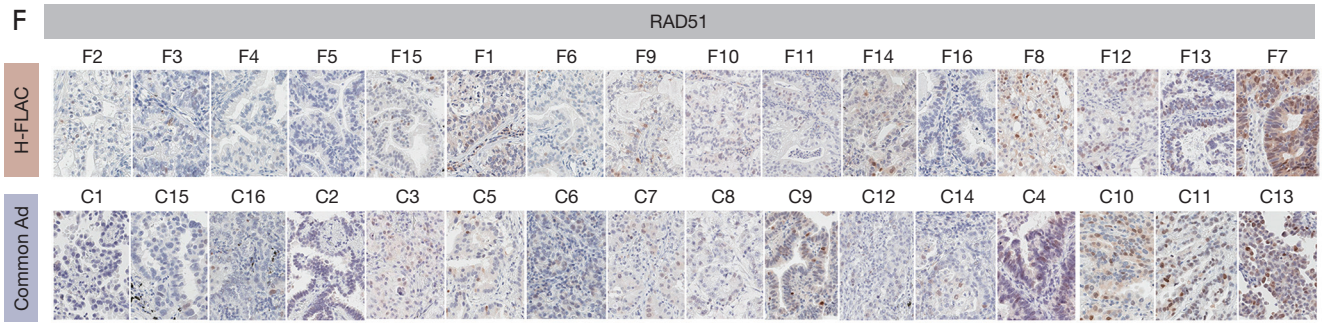

Figure 5 Immunohistochemical images of the fetal and common lung adenocarcinoma components. Expression of KMT2C (A), ATM (B), ATR (C), BRCA1 (D), and BRCA2 (E) tended to be lower in fetal components of the H-FLAC cases than in cancer tissues of the common adenocarcinoma cases (Common Ad). RAD51 tended to show low expression in all components (F). Immunohistochemical images for each marker are arranged from left to right in ascending order of expression. Magnification for each cell map: ×200. H-FLAC, high-grade fetal adenocarcinoma.

Table 2 Comparison of immunohistochemical scores between the fetal- and non-fetal-type components

Factors	P value
KMT2C	
H-FLAC *vs.* nonH-FLAC	0.44
H-FLAC *vs.* commonAd	0.02
ATM	
H-FLAC *vs.* nonH-FLAC	>0.99
H-FLAC *vs.* commonAd	0.02
ATR	
H-FLAC *vs.* nonH-FLAC	0.17
H-FLAC *vs.* commonAd	0.03
BRCA1	
H-FLAC *vs.* nonH-FLAC	0.27
H-FLAC *vs.* commonAd	0.18
BRCA2	
H-FLAC *vs.* nonH-FLAC	0.04
H-FLAC *vs.* commonAd	0.03
RAD51	
H-FLAC *vs.* nonH-FLAC	0.12
H-FLAC *vs.* commonAd	0.64

H-FLAC: the fetal-type component of the case F1–16; nonH-FLAC: the non-fetal-type adenocarcinoma component of the case F1–16; commonAd: common lung adenocarcinoma of the case C1–16. H-FLAC, high-grade fetal adenocarcinoma.

genes examined and in the pathway analysis of differentially expressed genes. This result could be partly due to small number of cases analysed and may further raise a possibility that low expression of *KMT2C* was caused both genetically and epigenetically. The third limitation is that we did not directly clarify the KMT2C regulatory effect on the expression of the HRR factors in lung cancers with an H-FLAC component. Thus, further studies are required to determine this function of KMT2C in H-FLAC using assays such as chromatin immunoprecipitation. In the future, clinical studies will be required to assess the efficacy of PARP inhibitors in lung cancers, including H-FLAC, with *KMT2C* mutation/low expression.

Comparison with similar researches

KMT2C mutations have been identified in various malignant tumours. Although studies in mice showed a tumour suppressor role of *KMT2C* in acute myeloid leukaemia and urothelial tumorigenesis (21,22), little is known about the consequences of *KMT2C* dysfunction in cancer cells. Recently, Rampias *et al.* reported that *KMT2C* knockdown caused decreased expression of HRR factors such as *ATM*, *ATR*, *BRCA1*, and *BRCA2* and increased sensitivity of urothelial cancer cells to the PARP inhibitor olaparib (13). In contrast, Chang *et al.* showed that KMT2C is recruited to the DNA damage site and directly mediates the HRR system through H3K4 methylation, chromatin relaxation, and secondary recruitment of HRR factors (23). It was also shown that both mutation and knockdown of *KMT2C* caused sensitization to olaparib in non-small

cell lung cancer cells (23). These findings suggest that *KMT2C* directly and/or indirectly promotes HRR, and *KMT2C* dysfunction is associated with sensitivity to PARP inhibitors. In our present study, RNA sequencing and immunohistochemical analyses showed that H-FLAC components showed lower expression of *KMT2C* and HRR factors than common lung adenocarcinomas, and *KMT2C* expression was positively correlated with the expression of HRR factors. Notably, RNA sequencing analysis showed strong correlations between the expression of KMT2C and HRR factors exclusively in H-FLACs but not in common adenocarcinomas. Our findings support the role of KMT2C as a positive regulator for the expression of HRR factors, which is compromised in H-FLACs.

As opposed to ovarian and breast cancers, in which the efficacy of PARP inhibitors is well studied (24,25), very few studies explore their efficacy in non-small-cell lung cancers. It was recently reported that knockdown of *ATM*, *BRCA1*, and *BRCA2* in non-small-cell lung cancer cells caused their hypersensitivity to olaparib (26). Although no clinical trials have demonstrated obvious therapeutic benefits of PARP inhibitors in non-small-cell lung cancers, a phase III trial of veliparib, a PARP inhibitor, in combination with platinum-based chemotherapy (NCT02106546) showed a favourable trend in lung squamous cell carcinomas with an LP52 signature, based on a 52-gene expression histology classifier (27). Hence, an appropriate case selection may contribute to the therapeutic benefits of PARP inhibitors in non-small-cell lung cancers. As H-FLACs rarely exhibit druggable mutations and PD-L1 expression (11), PARP inhibitors could be good therapeutic candidates for treatment of H-FLAC. Although there are few studies on RAD51 expression in lung cancers, high RAD51 expression was reported to be correlated with resistance to PARP inhibitors in germline BRCA-mutated breast cancers and ovarian cancers (28,29). The low RAD51 expression of H-FLACs may be a predictive finding for sensitivity to PARP inhibitors.

Although it was reported that inactivating mutations in HRR genes are associated with a high tumour mutation burden in breast cancer (30), H-FLACs showed a high tumour mutation burden in only 3/16 cases in our previous study (11). Therefore, unlike mutations, decreased expression of HRR genes may not contribute to an increase in mutation burden in H-FLAC. However, two of the three H-FLACs with a high tumour mutation burden exhibited low immunohistochemical expression (score 1+) of KMT2C, and the additional case harboured a nonsynonymous *KMT2C* mutation. Further studies of larger cohorts are required to elucidate an association between *KMT2C* mutation/low expression and tumour mutation burden in H-FLAC.

Our transcriptome analysis suggested that the Rho/Rac signalling pathway is inactivated as well. Rho/Rac GTPases regulate various cellular functions, including cell polarity, cell migration, and cell division (31). Notably, Rho GTPases play a key role in cancer cell invasion through dynamic regulation of actin cytoskeleton remodelling and cell adhesion. Recurrent gain-of-function mutations on RhoA have been reported in diffuse-type gastric carcinomas, characterised by a highly malignant phenotype with infiltrative invasion (32). However, the effect of Rho pathway inactivation on non-small-cell lung cancer has been unclear. Rho pathway inactivation might contribute to the formation of the fetal lung-like morphology and/or complex glandular structure in H-FLACs.

Explanations of findings

This study showed that *KMT2C* expression was significantly lower in H-FLACs than in common adenocarcinomas and was positively correlated with the expression of HRR factors.

Implications and actions needed

Our previous (11) and present studies suggest that the H-FLACs may be characterised by a high frequency of mutations and/or low expression of *KMT2C*. We speculate that H-FLACs with a high degree of *KMT2C* mutation/low expression may exhibit high sensitivity to PARP inhibitors. As we did not directly clarify the KMT2C regulatory effect on HRR factor expression, further studies are required to determine this function of KMT2C in H-FLAC using assays such as chromatin immunoprecipitation. Due to its rarity, more clinical studies of H-FLAC may not be realistic, but studies to assess the efficacy of PARP inhibitors in lung cancers based on stratification with *KMT2C* mutation/low expression are needed to improve therapeutic strategies and benefit H-FLAC patients.

Conclusions

H-FLAC components showed lower expression of *KMT2C* and HRR factors than common lung adenocarcinomas. *KMT2C* expression was positively correlated with the expression of HRR factors in lung adenocarcinomas. These

results support the hypothesis that loss of KMT2C function decreases the expression of the HRR factors in H-FLACs. We speculated that PARP inhibitors could be an effective drug for treatment of H-FLACs with *KMT2C* mutation/low expression.

Acknowledgments

We are grateful to the technical staff at Kanagawa Cancer Center for their expert technical assistance and the members of the Clinical Sequencing Team at Human Genome Center, Institute of Medical Science, The University of Tokyo, for their expert technical assistance and intellectual input. The super-computing resource was provided by the Human Genome Center, the Institute of Medical Science, The University of Tokyo (http://sc.hgc.jp/shirokane.html). Genomon 2 (https://github.com/Genomon-Project) was provided by Kenichi Chiba, Ai Okada, and Yuichi Shiraishi.
Funding: This work was supported in part by the Japan Society for the Promotion of Science (No. JP18K15111 to M.S., No. JP16H06276 to Y.M.).

Footnote

Reporting Checklist: The authors have completed the STROBE reporting checklist. Available at https://tlcr.amegroups.com/article/view/10.21037/tlcr-23-137/rc

Data Sharing Statement: Available at https://tlcr.amegroups.com/article/view/10.21037/tlcr-23-137/dss

Peer Review File: Available at https://tlcr.amegroups.com/article/view/10.21037/tlcr-23-137/prf

Conflicts of Interest: All authors have completed the ICMJE uniform disclosure form (available at https://tlcr.amegroups.com/article/view/10.21037/tlcr-23-137/coif). The authors have no conflicts of interest to declare.

Ethical Statement: The authors are accountable for all aspects of the work in ensuring that questions related to the accuracy or integrity of any part of the work are appropriately investigated and resolved. The study was conducted in accordance with the Declaration of Helsinki (as revised in 2013). The study was approved by the ethics committee of the Kanagawa Cancer Center (approval No. H28-Res60) in Yokohama, Japan, and individual consent for this retrospective analysis was waived.

References

1. Nakatani Y, Kitamura H, Inayama Y, et al. Pulmonary adenocarcinomas of the fetal lung type: a clinicopathologic study indicating differences in histology, epidemiology, and natural history of low-grade and high-grade forms. Am J Surg Pathol 1998;22:399-411.
2. WHO Classification of Tumours Editorial Board. Thoracic Tumours. 5th ed. Lyon: International Agency for Research on Cancer, 2021.
3. Sato S, Koike T, Yamato Y, et al. Resected well-differentiated fetal pulmonary adenocarcinoma and summary of 25 cases reported in Japan. Jpn J Thorac Cardiovasc Surg 2006;54:539-42.
4. Morita S, Yoshida A, Goto A, et al. High-grade lung adenocarcinoma with fetal lung-like morphology: clinicopathologic, immunohistochemical, and molecular analyses of 17 cases. Am J Surg Pathol 2013;37:924-32.
5. Zhang J, Sun J, Liang XL, et al. Differences between low and high grade fetal adenocarcinoma of the lung: a clinicopathological and molecular study. J Thorac Dis 2017;9:2071-8.
6. Suzuki M, Yazawa T, Ota S, et al. High-grade fetal adenocarcinoma of the lung is a tumour with a fetal phenotype that shows diverse differentiation, including high-grade neuroendocrine carcinoma: a clinicopathological, immunohistochemical and mutational study of 20 cases. Histopathology 2015;67:806-16.
7. Suzuki M, Nakatani Y, Ito H, et al. Pulmonary adenocarcinoma with high-grade fetal adenocarcinoma component has a poor prognosis, comparable to that of micropapillary adenocarcinoma. Mod Pathol 2018;31:1404-17.
8. Nakatani Y, Masudo K, Miyagi Y, et al. Aberrant nuclear localization and gene mutation of beta-catenin in low-grade adenocarcinoma of fetal lung type: up-regulation of the Wnt signaling pathway may be a common denominator for the development of tumors that form morules. Mod

Pathol 2002;15:617-24.
9. de Kock L, Bah I, Wu Y, et al. Germline and Somatic DICER1 Mutations in a Well-Differentiated Fetal Adenocarcinoma of the Lung. J Thorac Oncol 2016;11:e31-3.
10. Li Y, Xi SY, Yong JJ, et al. Morphologic, Immunohistochemical, and Genetic Differences Between High-grade and Low-grade Fetal Adenocarcinomas of the Lung. Am J Surg Pathol 2021;45:1464-75.
11. Suzuki M, Kasajima R, Yokose T, et al. Comprehensive molecular analysis of genomic profiles and PD-L1 expression in lung adenocarcinoma with a high-grade fetal adenocarcinoma component. Transl Lung Cancer Res 2021;10:1292-304.
12. Hu D, Gao X, Morgan MA, et al. The MLL3/MLL4 branches of the COMPASS family function as major histone H3K4 monomethylases at enhancers. Mol Cell Biol 2013;33:4745-54.
13. Rampias T, Karagiannis D, Avgeris M, et al. The lysine-specific methyltransferase KMT2C/MLL3 regulates DNA repair components in cancer. EMBO Rep 2019;20:e46821.
14. Heale JT, Ball AR Jr, Schmiesing JA, et al. Condensin I interacts with the PARP-1-XRCC1 complex and functions in DNA single-strand break repair. Mol Cell 2006;21:837-48.
15. Rouleau M, Patel A, Hendzel MJ, et al. PARP inhibition: PARP1 and beyond. Nat Rev Cancer 2010;10:293-301.
16. Alexander M, Kim SY, Cheng H. Update 2020: Management of Non-Small Cell Lung Cancer. Lung 2020;198:897-907.
17. Reck M, Rodríguez-Abreu D, Robinson AG, et al. Pembrolizumab versus Chemotherapy for PD-L1-Positive Non-Small-Cell Lung Cancer. N Engl J Med 2016;375:1823-33.
18. Wang Z, Jia R, Wang L, et al. The Emerging Roles of Rad51 in Cancer and Its Potential as a Therapeutic Target. Front Oncol 2022;12:935593.
19. Brierley JD, Gospodarowicz MK, Wittekind Ch. TNM Classification of Malignant Tumors. 8th ed. Hoboken, NJ: Wiley-Blackwell, 2017.
20. Sobin LH, Gospodarowicz MK, Wittekind Ch. TNM Classification of Malignant Tumors. 7th ed. Hoboken, NJ: Wiley-Blackwell, 2009.
21. Chen C, Liu Y, Rappaport AR, et al. MLL3 is a haploinsufficient 7q tumor suppressor in acute myeloid leukemia. Cancer Cell 2014;25:652-65.
22. Lee J, Kim DH, Lee S, et al. A tumor suppressive coactivator complex of p53 containing ASC-2 and histone H3-lysine-4 methyltransferase MLL3 or its paralogue MLL4. Proc Natl Acad Sci U S A 2009;106:8513-8.
23. Chang A, Liu L, Ashby JM, et al. Recruitment of KMT2C/MLL3 to DNA Damage Sites Mediates DNA Damage Responses and Regulates PARP Inhibitor Sensitivity in Cancer. Cancer Res 2021;81:3358-73.
24. Mirza MR, Coleman RL, González-Martín A, et al. The forefront of ovarian cancer therapy: update on PARP inhibitors. Ann Oncol 2020;31:1148-59.
25. Zimmer AS, Gillard M, Lipkowitz S, et al. Update on PARP Inhibitors in Breast Cancer. Curr Treat Options Oncol 2018;19:21.
26. Ji W, Weng X, Xu D, et al. Non-small cell lung cancer cells with deficiencies in homologous recombination genes are sensitive to PARP inhibitors. Biochem Biophys Res Commun 2020;522:121-6.
27. Ramalingam SS, Novello S, Guclu SZ, et al. Veliparib in Combination With Platinum-Based Chemotherapy for First-Line Treatment of Advanced Squamous Cell Lung Cancer: A Randomized, Multicenter Phase III Study. J Clin Oncol 2021;39:3633-44.
28. Cruz C, Castroviejo-Bermejo M, Gutiérrez-Enríquez S, et al. RAD51 foci as a functional biomarker of homologous recombination repair and PARP inhibitor resistance in germline BRCA-mutated breast cancer. Ann Oncol 2018;29:1203-10.
29. Feng Y, Wang D, Xiong L, et al. Predictive value of RAD51 on the survival and drug responsiveness of ovarian cancer. Cancer Cell Int 2021;21:249.
30. Mei P, Freitag CE, Wei L, et al. High tumor mutation burden is associated with DNA damage repair gene mutation in breast carcinomas. Diagn Pathol 2020;15:50.
31. Clayton NS, Ridley AJ. Targeting Rho GTPase Signaling Networks in Cancer. Front Cell Dev Biol 2020;8:222.
32. Kakiuchi M, Nishizawa T, Ueda H, et al. Recurrent gain-of-function mutations of RHOA in diffuse-type gastric carcinoma. Nat Genet 2014;46:583-7.

Cite this article as: Suzuki M, Kasajima R, Yokose T, Shimizu E, Hatakeyama S, Yamaguchi K, Yokoyama K, Katayama K, Yamaguchi R, Furukawa Y, Miyano S, Imoto S, Shinozaki-Ushiku A, Ushiku T, Miyagi Y. *KMT2C* expression and DNA homologous recombination repair factors in lung cancers with a high-grade fetal adenocarcinoma component. Transl Lung Cancer Res 2023;12(8):1738-1751. doi: 10.21037/tlcr-23-137

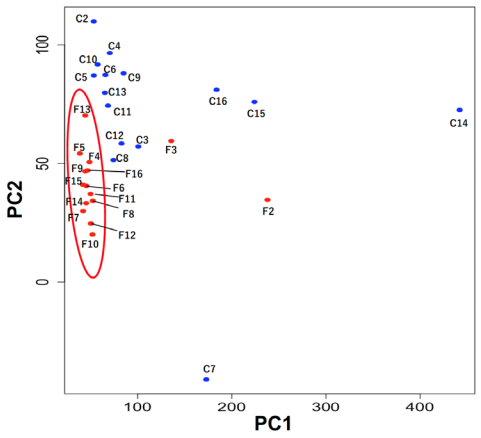

Figure S1 PCA analysis of the gene expression profile of high-grade fetal adenocarcinoma (H-FLAC) and the common adenocarcinoma counterpart of the lung. Each H-FLAC case (F2-16) is indicated by a red dot, whereas the common adenocarcinoma cases (C1-16) are shown by the blue dots with case identification numbers (see text). Cases of H-FLAC located close to each other are encircled in red, indicating a close group of 13 out of 15 H-FLAC cases examined. PCA, principal component analysis.

Table S1 Predicted pathways by IPA with P-value less than 0.05, corresponding to -log (P-value) greater than 1.3

Pathways	–log (P-value)	Ratio	z-score	molecules encoded by the DEGs involved in the constituents of the pathway
Role of BRCA1 in DNA Damage Response	5.02E+00	1.75E–01	–1.89	ACTB, ARID1A, ARID2, ATR, BLM, CHEK2, FANCD2, FANCM, MRE11, MSH2, NBN, RFC1, SMARCC1, STAT1
Complement System	4.71E+00	2.50E–01	–0.378	C1R, C1S, C3, C5, C6, CD55, CFI, ITGB2, SERPING1
Hereditary Breast Cancer Signaling	3.87E+00	1.22E–01	NaN	ACTB, ARID1A, ARID2, ATR, BLM, CHEK2, FANCD2, FANCM, MRE11, MSH2, NBN, PIK3R3, PIK3R4, POLR2B, RFC1, SMARCC1, UBC
Cell Cycle: G2/M DNA Damage Checkpoint Regulation	3.53E+00	1.80E–01	0.378	ATR, CHEK2, MDM2, SKP1, TOP2A, TRIP12, YWHAE, YWHAG, YWHAQ
RhoA Signaling	3.51E+00	1.23E–01	–2.496	ABL2, ACTB, ACTR2, ARHGAP35, ARHGEF12, ARPC1A, CFL2, NEDD4, NGEF, NRP2, PIP5K1B, PTK2, RAPGEF2, RDX, RHPN2
Serotonin and Melatonin Biosynthesis	3.10E+00	6.00E–01	NaN	ASMT, TPH1, TPH2
Clathrin-mediated Endocytosis Signaling	3.06E+00	9.90E–02	NaN	ACTB, ACTR2, AP3B1, AP3M1, APOB, ARPC1A, CBL, CLTA, DAB2, EGF, HSPA8, ITGB1, ITGB2, MDM2, PIK3R3, PIK3R4, SYNJ1, TSG101, UBC
Mitotic Roles of Polo-Like Kinase	2.77E+00	1.43E–01	–2.449	ANAPC1, ANAPC4, CDC16, CDC23, CHEK2, PLK4, PPP2CB, PPP2R5C, SLK
DNA Double-Strand Break Repair by Homologous Recombination	2.58E+00	2.86E–01	NaN	ATRX, GEN1, MRE11, NBN
ATM Signaling	2.48E+00	1.15E–01	–1	ATR, BLM, CHEK2, FANCD2, MAPK8, MDM2, MRE11, NBN, PPP2CB, PPP2R5C, SMC2
Role of CHK Proteins in Cell Cycle Checkpoint Control	2.47E+00	1.40E–01	–2.646	ATR, CHEK2, MRE11, NBN, PPP2CB, PPP2R5C, RAD1, RFC1
HIPPO signaling	2.42E+00	1.19E–01	1.414	DLG5, ITCH, PPP2CB, PPP2R5C, SKP1, STK3, STK4, YWHAE, YWHAG, YWHAQ
Rac Signaling	2.12E+00	9.49E–02	–3.464	ACTR2, ARPC1A, CFL2, CYBB, IQGAP1, ITGB1, ITGB2, MAPK8, NCKAP1, PIK3R3, PIK3R4, PIP5K1B, PTK2
MSP-RON Signaling In Cancer Cells Pathway	2.12E+00	9.49E–02	–2.887	BRAF, ELF1, HNF1A, ITGB1, PIK3R3, PIK3R4, PTK2, RPS6KA3, SOS2, TCF4, YWHAE, YWHAG, YWHAQ
Protein Ubiquitination Pathway	2.06E+00	7.78E–02	NaN	ANAPC1, ANAPC4, CBL, CDC23, DNAJC21, DNAJC8, HSPA8, MDM2, NEDD4, PSMA3, PSMC6, PSMD9, SKP1, TRAF6, UBC, UBE2Q1, UBE3A, UBR1, USO1, USP36, USP9Y
Actin Cytoskeleton Signaling	1.99E+00	7.92E–02	–2.5	ACTB, ACTR2, ARHGAP35, ARHGEF12, ARPC1A, CFL2, EGF, IQGAP1, ITGB1, ITGB2, NCKAP1, PIK3R3, PIK3R4, PIP5K1B, PTK2, RDX, SOS2, TLN1, TRIO
EGF Signaling	1.99E+00	1.27E–01	–2.646	EGF, ITPR2, MAPK8, PIK3R3, PIK3R4, SOS2, STAT1
p53 Signaling	1.95E+00	1.02E–01	0.378	ATR, CCNG1, CHEK2, MAPK8, MDM2, PIK3R3, PIK3R4, ST13, STAG1, TRIM29
EIF2 Signaling	1.89E+00	8.02E–02	–1.897	ACTB, EIF2AK3, EIF3E, EIF3H, EIF4G3, PIK3R3, PIK3R4, RPL23, RPL32, RPL34, RPL37, RPLP0, RPS24, RPS3, RPS4Y1, SOS2, WARS1
ERK/MAPK Signaling	1.87E+00	7.98E–02	–1.941	BRAF, ELF1, ITGB1, ITGB2, KSR1, LAMTOR3, MKNK2, PIK3R3, PIK3R4, PPP2CB, PPP2R5C, PTK2, SOS2, STAT1, TLN1, YWHAG, YWHAQ
Signaling by Rho Family GTPases	1.86E+00	7.55E–02	–4	ACTB, ACTR2, ARHGEF12, ARPC1A, CDH12, CDH9, CFL2, CLIP1, CYBB, GNAZ, IQGAP1, ITGB1, ITGB2, MAPK8, NEDD4, PIK3R3, PIK3R4, PIP5K1B, PTK2, RDX

Table S1 *(continued)*

https://dx.doi.org/10.21037/tlcr-23-137

Table S1 *(continued)*

Pathways	–log (P-value)	Ratio	z-score	molecules encoded by the DEGs involved in the constituents of the pathway
UDP-N-acetyl-D-galactosamine Biosynthesis II	1.86E+00	2.50E–01	NaN	GNPDA2, GNPNAT1, GPI
Acute Phase Response Signaling	1.79E+00	8.15E–02	–1.897	C1R, C1S, C3, C5, ELP1, HNF1A, IL18, IL6ST, MAPK8, PIK3R3, SERPING1, SOD2, SOS2, TCF4, TRAF6
IGF-1 Signaling	1.78E+00	9.62E–02	–2.236	IGFBP4, MAPK8, NEDD4, PIK3R3, PIK3R4, PTK2, SOS2, YWHAE, YWHAG, YWHAQ
Ephrin A Signaling	1.78E+00	1.28E–01	NaN	ADAM10, CFL2, NGEF, PIK3R3, PIK3R4, PTK2
IL-15 Production	1.77E+00	9.17E–02	–2.714	ABL2, KDR, LMTK2, MERTK, PTK2, ROR2, ROS1, STAT1, TNK2, TWF1, TXK
TCA Cycle II (Eukaryotic)	1.71E+00	1.67E–01	–2	OGDH, SDHA, SLC35G3, SUCLG1
Leukocyte Extravasation Signaling	1.69E+00	7.94E–02	–2.887	ACTB, ARHGAP35, CLDN14, CYBB, F11R, ITGB1, ITGB2, MAPK8, MMP10, PIK3R3, PIK3R4, PTK2, RDX, SELPLG, TXK
GP6 Signaling Pathway	1.67E+00	8.87E–02	–2.714	ADAM10, COL1A2, COL3A1, COL6A5, COL9A1, LAMA1, LAMC1, PIK3R3, PIK3R4, PTK2, TLN1
Zymosterol Biosynthesis	1.59E+00	3.33E–01	NaN	CYP51A1, LBR
PI3K/AKT Signaling	1.55E+00	7.61E–02	–1.155	ELP1, GYS2, IL6ST, ITGB1, ITGB2, MDM2, PIK3R3, PPP2CB, PPP2R5C, RHEB, SOS2, SYNJ1, YWHAE, YWHAG, YWHAQ
3-phosphoinositide Biosynthesis	1.53E+00	7.58E–02	–3.606	FIG4, PIK3R3, PIK3R4, PIP5K1B, PP2D1, PPP2CB, PPP2R5C, PTPN1, PTPN13, PTPN22, PTPRC, PTPRJ, SYNJ1, TPTE2, UBLCP1
Lymphotoxin b Receptor Signaling	1.51E+00	1.11E–01	–2.449	CYCS, ELP1, PIK3R3, PIK3R4, TRAF5, TRAF6
FAK Signaling	1.49E+00	8.62E–02	NaN	ACTB, ARHGAP26, EGF, ITGB1, ITGB2, PIK3R3, PIK3R4, PTK2, SOS2, TLN1
CNTF Signaling	1.44E+00	1.07E–01	–2.449	IL6ST, PIK3R3, PIK3R4, RPS6KA3, RPS6KA6, STAT1
Senescence Pathway	1.43E+00	6.80E–02	–2.84	ANAPC1, ANAPC4, ATR, BRAF, CACNA2D1, CDC16, CDC23, CHEK2, ELF1, EP400, ITPR2, MDM2, MRE11, NBN, PIK3R3, PIK3R4, PPP2CB, PPP2R5C, SOD2, TRAF6
ERK5 Signaling	1.41E+00	9.72E–02	–2.646	EGF, IL6ST, RPS6KA3, RPS6KA6, YWHAE, YWHAG, YWHAQ
Virus Entry via Endocytic Pathways	1.40E+00	8.65E–02	NaN	ACTB, AP3B1, AP3M1, CD55, CLTA, ITGB1, ITGB2, PIK3R3, PIK3R4
Regulation of Cellular Mechanics by Calpain Protease	1.40E+00	9.09E–02	NaN	CNGA3, CNGB1, CNGB3, EGF, ITGB1, ITGB2, PTK2, TLN1
RANK Signaling in Osteoclasts	1.37E+00	8.99E–02	–2.646	CBL, ELP1, MAPK8, MITF, PIK3R3, PIK3R4, TRAF5, TRAF6
Superpathway of Inositol Phosphate Compounds	1.35E+00	7.05E–02	–3.742	FIG4, PIK3R3, PIK3R4, PIP5K1B, PP2D1, PPIP5K2, PPP2CB, PPP2R5C, PTPN1, PTPN13, PTPN22, PTPRC, PTPRJ, SYNJ1, TPTE2, UBLCP1
Paxillin Signaling	1.35E+00	8.49E–02	–2.828	ACTB, ITGB1, ITGB2, MAPK8, PIK3R3, PIK3R4, PTK2, SOS2, TLN1
Ceramide Signaling	1.35E+00	8.89E–02	–1.134	CYCS, KSR1, MAPK8, NSMAF, PIK3R3, PIK3R4, PPP2CB, PPP2R5C
NRF2-mediated Oxidative Stress Response	1.33E+00	7.11E–02	–2.449	ABCC2, ACTB, AKR7A2, AOX1, DNAJC21, DNAJC8, EIF2AK3, FKBP5, GCLC, HACD3, MAPK8, MGST2, PIK3R3, PIK3R4, SOD2
Regulation of eIF4 and p70S6K Signaling	1.33E+00	7.43E–02	–0.816	EIF3E, EIF3H, EIF4G3, ITGB1, ITGB2, PIK3R3, PIK3R4, PPP2CB, PPP2R5C, RPS24, RPS3, RPS4Y1, SOS2
Inhibition of ARE-Mediated mRNA Degradation Pathway	1.31E+00	7.55E–02	–0.333	DDX6, PPP2CB, PPP2R5C, PSMA3, PSMC6, PSMD9, PSME4, TNFSF10, XRN1, YWHAE, YWHAG, YWHAQ

Identified IPA pathways are listed in descending order of the -log (P-value). Ratio, numbers of DEGs in the pathway was divided by that of genes included the pathway; z-score, negative z-scores indicates inactivation and vice versa. NaN means ineligible for analysis to assign the score.

https://dx.doi.org/10.21037/tlcr-23-137

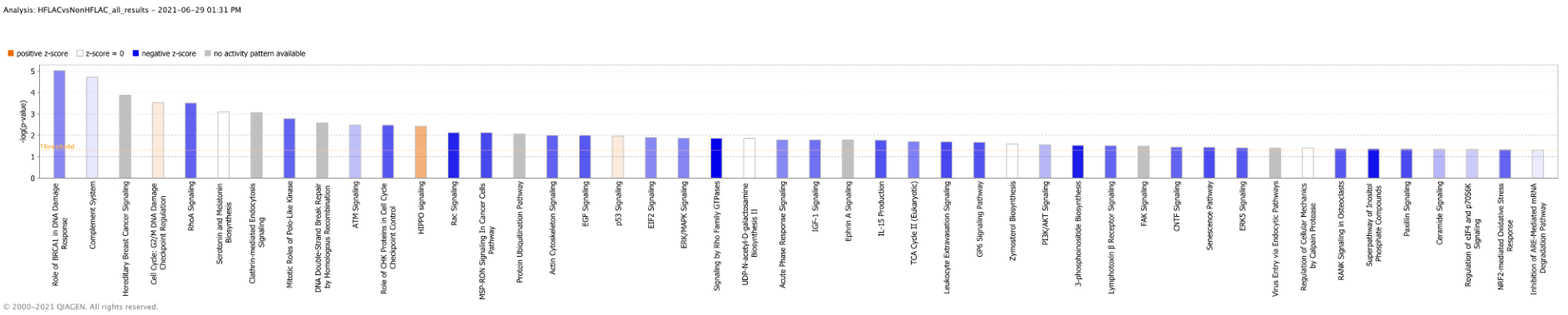

Figure S2 All 46 IPA pathways with a significant association with DEGs in high-grade fetal adenocarcinoma and common adenocarcinoma. The drawing was made through the IPA analysis, provided by the Ingenuity systems, QIAGEN. IPA, ingenuity pathway analysis; DEGs, differentially expressed genes.

A

19 DEGs
Gene Symbol
AGAP11
BEND3
C21orf91
CATSPER3
CNNM2
CSMD1
DGCR6
FIBIN
GRB10
KRT6C
MTPAP
MUC2
MUC3A
NTSR1
PLEKHA7
TBC1D26
VCX3B
DKFZP434K028
LOC728888

B

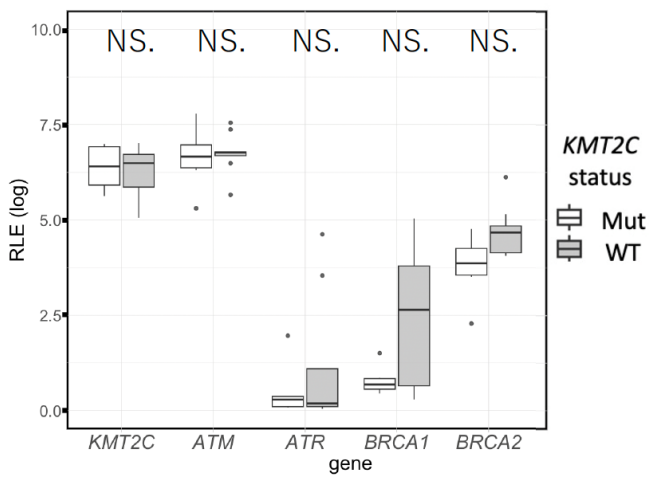

Figure S3 Comparison between high-grade fetal adenocarcinomas (H-FLACs) with and without *KMT2C* mutation. Gene expression obtained by RNA sequencing of six H-FLACs with *KMT2C* mutation was compared with ones without the mutations. (A) Symbols of 19 genes identified as DEGs. (B) Comparison of expression of *KMT2C*, *ATM*, *ATR*, *BRCA1*, and *BRCA2*. Boxplots were provided just as the ones in *Figure 3*. NS, non-significant; Mut, *KMT2C* mutation; WT, *KMT2C* wild type; DEGs, differentially expressed genes.

https://dx.doi.org/10.21037/tlcr-23-137

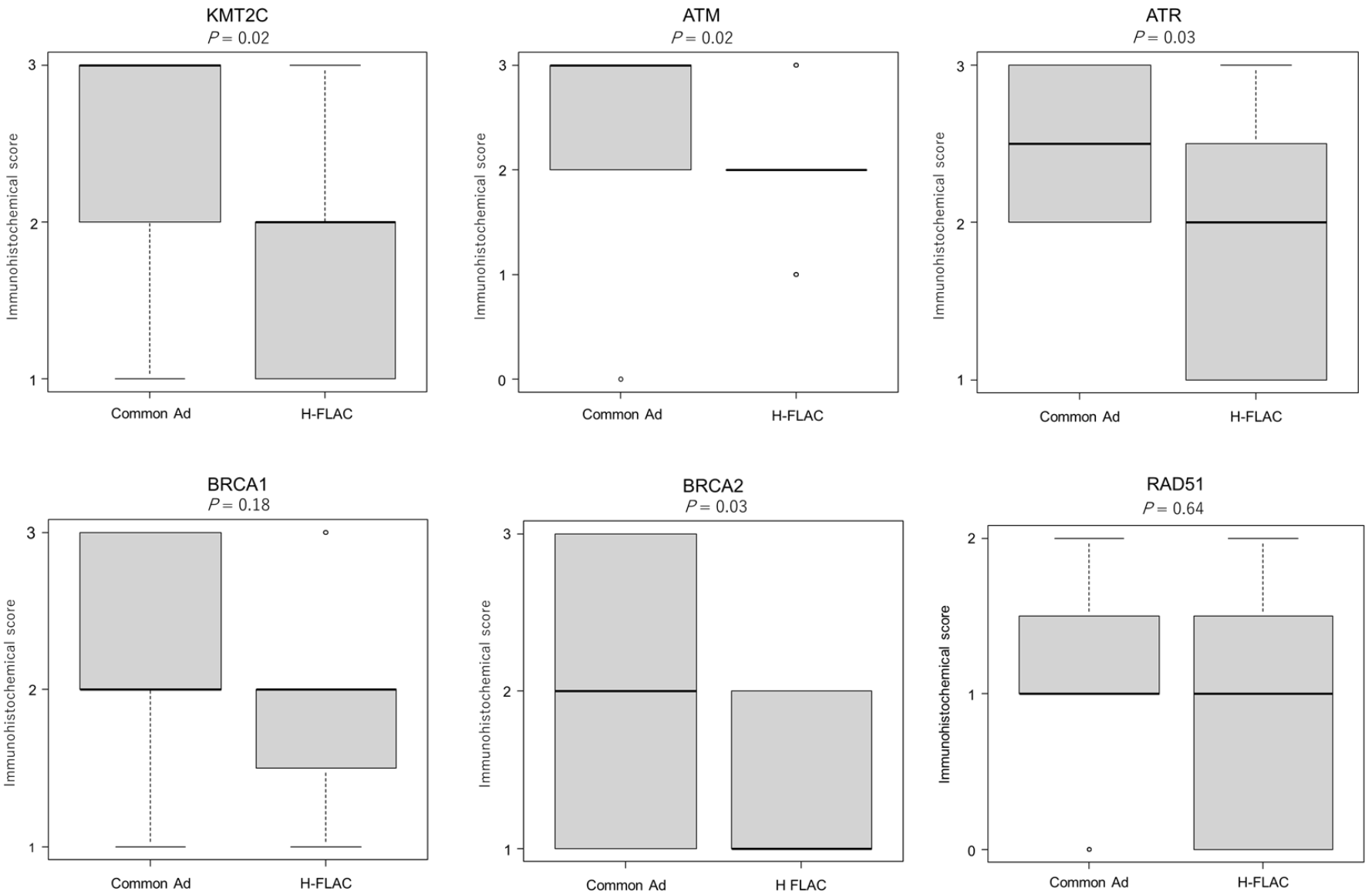

Figure S4 Boxplots of immunohistochemical expressions of KMT2C and HRR factors. Boxes indicate the first and the third quartile counts, lines in boxes indicate median values, and ends of whiskers indicate minimum and maximum values respectively. Dots demonstrate outliers. Common Ad, common adenocarcinoma; H-FLAC, high-grade fetal adenocarcinoma; HRR, homologous recombination repair.

https://dx.doi.org/10.21037/tlcr-23-137